CHAPTER

Advances in Fiber Distributed-Feedback Lasers

1

Michalis N. Zervas
Optoelectronics Research Centre, University of Southampton, Southampton SO17 1BJ, UK

1.1 INTRODUCTION

The recent re-introduction of optical coherent techniques has revolutionized modern telecom communications and has resulted in the most spectrally efficient optical system demonstrations to date [1]. In addition to record spectral efficiencies, coherent communication systems offer other advantages in terms of system flexibility, reduced signal-to-noise ratio requirements, increased resilience against fiber chromatic dispersion and in many aspects simplify the system design. However, coherent detection systems, such as, for example, coherent-optical orthogonal-frequency-division-multiplexed (CO-OFDM) systems, and advanced modulation formats, such as quadrature amplitude modulation (QAM), impose much more stringent requirements on source linewidth, stability, and phase/frequency noise characteristics. The development of inexpensive laser sources, with high coherence and stability, is expected to replace expensive external-cavity semiconductor lasers and allow their use as local oscillators similar to the way local oscillators are used in today's radio communication systems. The performance of CO-OFDM is in general 3 dB better than that of incoherent OFDM since no optical power is allocated for the carrier. However, CO-OFDM requires a laser at the receiver to generate the carrier locally. It is, therefore, more sensitive to phase noise and the main challenge of CO-OFDM is that the phase noise of the local oscillator must be compensated for. It has been shown that the influence of phase noise can be reduced by using lasers with narrow linewidth [2,3].

So far, practical commercial telecommunication systems are almost entirely based on semiconductor-based lasers as their optical sources, because of their compact size, high speed and reliability, and direct electronic control. Over the past decade, continuous-wave and pulsed fiber lasers, covering a quite large spectral window, have experienced a remarkable progress and have penetrated successfully quite diverse industrial sectors. Also, a number of different fiber lasers, such as ultrashort, ultrafast, or frequency stabilized ring lasers, operating in the telecom window have already been used extensively in a number of coherent system demonstrators [4]. In addition, fiber distributed-feedback (DFB) laser technology has matured considerably

Optical Fiber Telecommunications VIA. http://dx.doi.org/10.1016/B978-0-12-396958-3.00001-9

and various sectors, such as the optical sensor sector, have benefited enormously from their unique characteristics, such as their robustness, electromagnetic-radiation immunity, power scalability, narrow linewidth, and exceptional phase-noise performance. A review of the high-performance fiber DFB lasers and their potential use in future high spectral efficiency telecom systems, in particular, is timely. This chapter covers advances in fiber DFB lasers and their potential use in modern telecom systems. It considers different designs and configurations and their impact on the laser performance. Special emphasis is given to power scalability and stability, linewidth, and phase/frequency noise characteristics. A brief comparison with other technologies in the telecom and non-telecom applications space is also given. The chapter concludes with a summary and an outlook of the fiber laser technologies and the future prospects.

1.2 FIBER DFB LASERS

1.2.1 Introduction

DFB lasers were first proposed and demonstrated by Kogelnik and Shank [5,6]. In DFB laser cavities; feedback is provided by distributed Bragg structures, instead of classic discrete mirrors, resulting in compact and frequency-stable devices. The first demonstration involved a UV-exposed periodic structure on a gelatin film soaked in a dye (rhodamine 6G). This was followed by demonstrations of optically and electrically pumped DFB lasers with semiconductor (GaAs) active materials and ion-milled corrugated waveguides [7,8]. The first demonstrations involved waveguide corrugations; corresponding to uniform periodic effective-index variations (see Figure 1.1a). The mode spectrum of such periodic structures exhibits a gap around the Bragg wavelength, with equal threshold modes λ_1 and λ_2 occurring symmetrically on either side of the gap. This threshold degeneracy results in frequency instabilities and compromises the use of such devices in telecom and other high-performance applications. To overcome this problem, Haus and Shank [9] suggested the introduction of an antisymmetric variation of the periodic index modulation. This can be practically achieved by the insertion of a quarter-wavelength (QW) section ($\lambda_0/4n_{\text{eff}} = \Lambda/2$)—or equivalently π-phase-shift—between two equal uniform DFB structures (see Figure 1.1b). This "defect" allows the existence of a mode within the stopband of the uniform sections, with the field decaying exponentially from the center into the gratings on either side. Compared to uniform DFB structures, this mode has lower threshold and higher stability when used in a laser cavity. This quarter-wavelength phase slip in the middle of the RI modulation profile essentially turns the uniform DFB structure into an effective Fabry-Perot cavity of length L_{eff}. Due to symmetry, the symmetric QW-shifted DFB is bidirectional with almost equal powers emitted from both laser ends. Unidirectionality can be achieved by moving the QW shift closer to one end [10], as shown schematically in Figure 1.1c. In this case, the length of the effective FP cavity remains largely unchanged and the overall

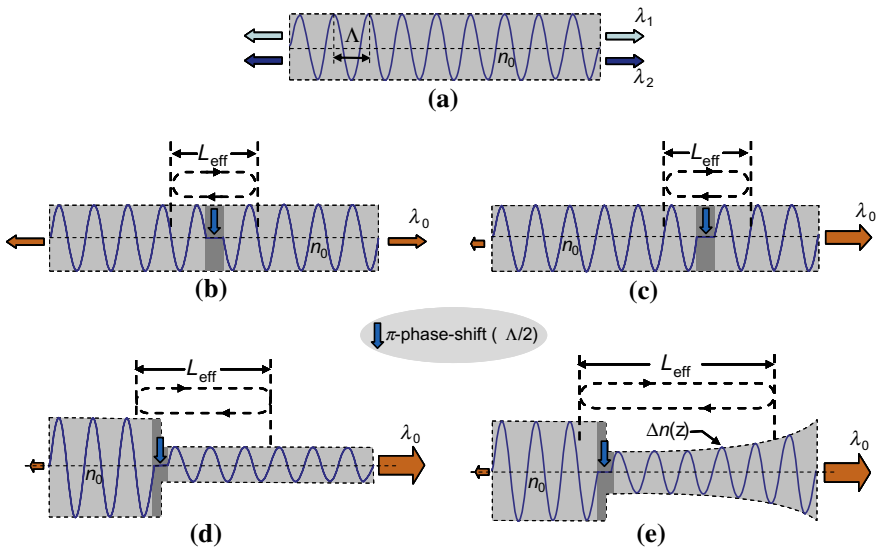

FIGURE 1.1 Symmetric and asymmetric DFB laser refractive index profiles: (a) uniform variation, (b) symmetric π-phase-shifted, (c) asymmetric π-phase-shifted, (d) step-apodized, asymmetric π-phase-shifted, and (e) optimized-apodization asymmetric π-phase-shifted.

power extraction efficiency remains almost constant. However, the forward/backward power ratio improves considerably.

1.2.2 Fiber π-phase-shifted DFB lasers

The basic DFB fiber laser configuration is shown schematically in Figure 1.2a. It consists of a length of doped fiber within which a phase-shifted Bragg grating is inscribed. Each end of the doped fiber is spliced to a passive fiber and the DFB laser is pumped through a WDM coupler in a co-directional (Figure 1.2b) or counter-directional (Figure 1.2c) pumping scheme.

Early fiber DFB lasers focused on the important 1.5 μm telecom window. The first fiber DFB laser demonstration used a single Bragg grating at 1.5 μm written directly into a 2 cm-long Er^{3+}/Yb^{3+}-doped fiber. Robust single-frequency operation was achieved by locally heating the center of the grating to create the necessary phase shift [11]. Robust single-mode operation was achieved with an Er^{3+}-doped DFB fiber laser based on a 36 mm-long Bragg grating with a permanently UV-induced $\pi/2$ phase-shift, yielding an output power of 5.4 mW and a linewidth of 15 kHz [12]. A number of different DFB lasers followed using either Er^{3+} or Er^{3+}/Yb^{3+}-codoped fibers [13,14]. In order to avoid clustering, Er^{3+}-doped fibers are usually of low concentration and result in low efficiencies (a few %) and relatively low output powers

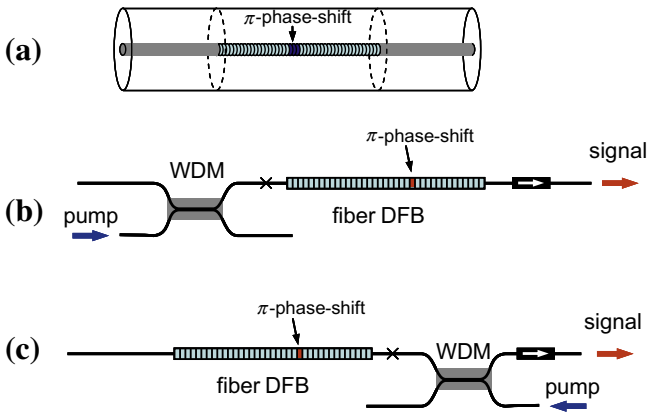

FIGURE 1.2 (a) Fiber DFB laser schematic and typical, (b) co-, and (c) counter-pumping schemes.

(a few mW). Yb^{3+} codoping results in much more efficient pump absorption and gives increased efficiencies (tens of %) and larger output powers (tens of mW).

1.2.2.1 Grating writing techniques

Grating writing techniques are essential in developing robust, high-performance fiber DFB lasers. Their modal and polarization performance depends critically on the writing beam characteristics. Fiber DFB laser fabrication is based primarily on well-established ultraviolet (UV) light fiber-Bragg grating writing techniques [15]. They use predominantly Argon-ion 244 nm lasers, because of their superior stability and beam quality, to either directly scan phase masks—with all the apodization and phase characteristics designed in—or multiple "exposure-and-shift" techniques, which provide more flexibility and versatility [16]. The aforementioned techniques require specially prepared and photo-sensitized fiber and somehow limit the range of fibers that can be ultimately used. Lately other grating inscribing techniques have been developed which rely on femtosecond pulsed lasers in the near infrared and do not require special photosensitive fibers [17], opening up almost endless possibilities in terms of candidate fiber host materials and geometries.

1.2.2.2 Novel fiber DFB cavity designs

Despite the performance improvements achieved by the introduction of the center or off-center π-phase-shift, uniform DFB lasers are still sub-optimum, in that the gain medium is not utilized effectively throughout its length and the power extraction efficiency as well as the side-mode suppression are reduced. The directionality and power extraction efficiency can be improved further by using novel step-apodized, π-phase-shifted refractive-index profiles [18] or optimized π-phase-shifted structures

with ultimate efficiency [19], where the extraction efficiency is maximized over the entire laser length.

1.2.2.2.1 Step-apodized, asymmetric π-phase-shifted designs

Propagation in an active fiber with periodically modified core refractive index $n(z) = n_0 + \Delta n(z)\cos[(2\pi/\Lambda)z + \phi]$, with period Λ and refractive index change profile $\Delta n(z)$ (see Figure 1.1), is described by the standard coupled-mode equations for the two counter-propagating field amplitudes $R_+(z)$ and $R_-(z)$ [19], namely:

$$\frac{dR_+(z)}{dz} = +\alpha(z)R_+(z) + \kappa(z)R_-(z)\exp(+i\Phi z), \tag{1.1}$$

$$\frac{dR_-(z)}{dz} = -\alpha(z)R_-(z) + \kappa(z)R_+(z)\exp(-i\Phi z). \tag{1.2}$$

In the equations above, $\alpha(z)$ is the gain distribution, $\kappa(z) \approx (\pi/\lambda)\Delta n(z)$ is the coupling constant, $\Phi = 2(\beta - \pi/\Lambda)$, β is the propagation constant, and λ is the free-space wavelength. In a uniform grating, when $\alpha \ll \kappa$ (as is the case in practical fiber DFBs) the effective penetration depth at the Bragg wavelength ($\lambda_B = 2n_0\Lambda$) is approximated by $d \approx \tanh(\kappa L)/(2\kappa)$. By changing the grating strengths κ_1 and κ_2 and lengths L_1 and L_2 of the uniform gratings on either side of the phase shift, as shown schematically in Figure 1.1d, the effective cavity length d_T, defined as the sum of effective penetration depths ($d_T = d_1 + d_2$), is increased and, in addition to uni-directionality, the asymmetric DFB laser shows enhanced efficiency. Figure 1.3a shows that in comparison with the uniform asymmetric phase-shift design, when the phase shift is moved toward the input end, the step-apodized effective cavity length increases by ~23% and the output power increases by ~33%. The proportionally larger increase in output power is due to the fact that in addition to the effective cavity length increase, the step-apodized designs result in better overall saturation and larger extraction efficiency.

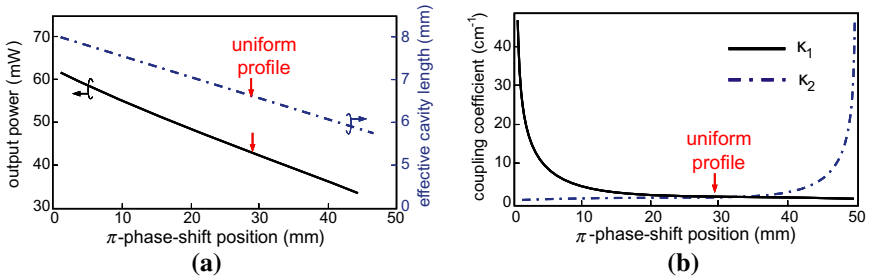

FIGURE 1.3 (a) Output power and effective cavity lengths and (b) required grating strengths as a function of π-phase-shift position (the arrows indicate the parameters of the optimum uniform design).

The active fiber length is kept constant in all cases. Figure 1.3b plots the required variation of the grating coupling constants showing that the maximum improvements require extremely strong gratings on the input side. Such strengths are not possible with common grating writing techniques and achievement of the maximum efficiencies might require use of butt-coupled mirrors or spliced external passive gratings [20].

Figure 1.4a and b shows the threshold gain for the fundamental mode and gain margins with respect to the second-order side modes, respectively, for step-apodized fiber DFBs, as a function of π-phase-shift position. They also include the corresponding parameters for a uniform DFB without phase shift and with optimized π-phase-shift. All lasers have the same length and optimum coupling constants. It is shown that compared to uniform structures with asymmetrically placed π-phase-shift, the step-apodized designs show lower threshold for the fundamental lasing mode and substantially increased gain margins. The uniform DFB structure with no phase shift shows the lowest threshold, but as already mentioned it is bidirectional and dual-wavelength and, therefore, of limited practical use. The gain margins of the step-apodized design are larger than the other two configurations.

Figure 1.5a and b compares the internal gain and signal power distribution for the conventional uniform asymmetric and step-apodized π-phase-shifted designs. The corresponding grating strengths are shown in Figure 1.3b. It is evident that the step-apodized design shows a larger saturated area and it is expected to have higher efficiency. Figure 1.5c, on the other hand, shows the corresponding pump power distribution and the positions of effective reflections and delineates the areas of the resulting effective cavities. It is realized that in the case of the step-apodized design not only the effective cavity is longer (7.4 mm as opposed to 6.6 mm in the case of uniform profile), but there is also more pump power delivered at the effective cavity area. Finally, due to the higher saturation more pump power is absorbed. The combination of all these effects results in the aforementioned efficiency increase.

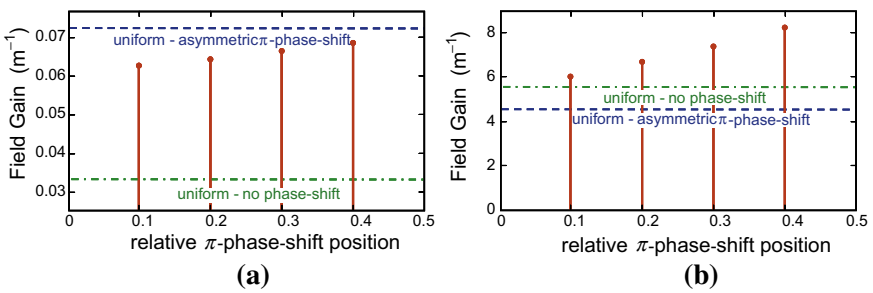

FIGURE 1.4 (a) Fundamental mode threshold gain and (b) threshold gain margin as a function of π-phase-shift position. Uniform DFB without phase shift and with optimized π-phase-shift are also shown for comparison.

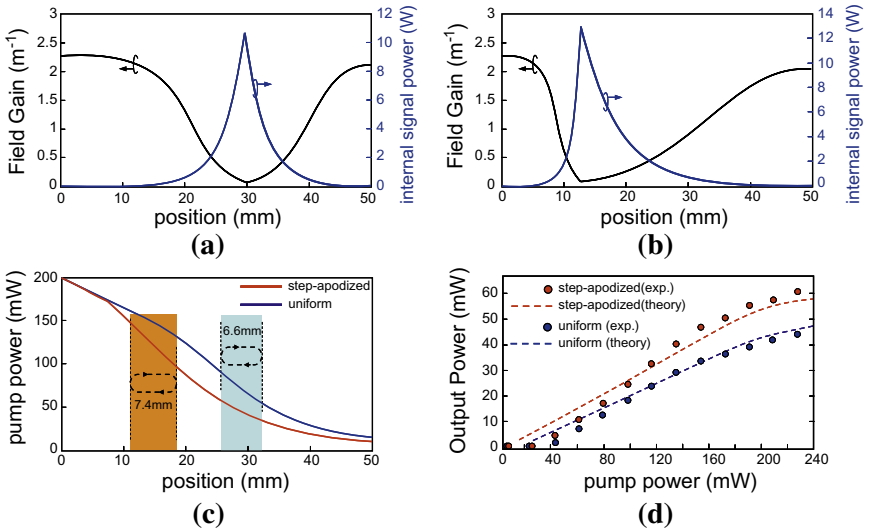

FIGURE 1.5 Internal gain and signal power distribution for (a) conventional uniform asymmetric and (b) step-apodized π-phase-shifted designs, (c) corresponding pump power distribution and the positions of effective reflections and effective cavities, and (d) experimental results (from [18]).

We applied experimentally the step-apodized design approach in an Er^{3+}/Yb^{3+}-codoped fiber and compared it to a conventional uniform asymmetric design. The alumino-phospho-silicate fiber core was surrounded by a photosensitive germano-silicate ring doped with boron, matching the refractive index of the silica cladding. The core radius of the fiber was 2.3 μm and the cut-off wavelength was 1150 nm, giving NA = 0.19. The refractive index grating was written in the photosensitive ring by exposing the fiber to ultraviolet interference pattern produced by a phase mask. The optimum coupling coefficient and phase-shift position for maximum unidirectional output of the uniform profile were experimentally found to be 1.53 cm^{-1} and 29 mm, respectively, for a 50 mm-long device. These experimental results are in very good agreement with the simulation predictions. Using these values for a 50 mm-long step-apodized DFB profile, the optimum phase-shift position was calculated to be ~12.5 mm. Figure 1.5d compares the experimental and theoretical output power variation with input pump power for two fiber DFB lasers. It is shown that the step-apodized design results in ~33% efficiency increase, in close agreement with the theory.

1.2.2.3 Inverse-engineered designs with ultimate efficiency

So far, the optimum values of phase shift and grating coupling constant are found through a *parametric optimization* process of an a priori defined cavity by varying the parameters over predetermined ranges, either by simulation or by experimentation.

It has been shown that the efficiency increase achieved, in particular by the step-apodized designs, was primarily a result of the larger effective cavity length and overall saturation. However, even in these superior designs, optimum saturation and extraction efficiency were achieved only over, albeit increased, a still relatively small part of the cavity. In this section, we consider an *inverse-engineered* analytical approach to design fiber DFB cavities with optimum saturation *throughout* the cavity length, providing *ultimate* extraction efficiency. In this approach, for a given pump power and pumping geometry, we first define the optimum pump and signal distributions along the entire active medium length, which give maximum power extraction efficiency throughout. We then use these distributions to design the generalized distributed-feedback cavity that produces the optimum signal power distribution in one step.

By introducing the average signal intensity $S = R_+^2 + R_-^2$ and intensity difference $D = R_+^2 - R_-^2$, the standard propagation Eqs. (1.1) and (1.2) can be put in the following form [19]:

$$D(z) = D(0) + 2\int_0^z \alpha(z')S(z')dz', \tag{1.3}$$

$$\kappa(z) = \frac{1}{\sqrt{S(z)^2 - D(z)^2}}\left(\frac{1}{2}\frac{dS(z)}{dz} + D(z)\alpha(z)\right)\left\{\cos\left[\left(2\beta - \frac{2\pi}{\Lambda(z)}\right)\right]\right\}^{-1}. \tag{1.4}$$

Equations (1.3) and (1.4) constitute the basis of the new design method. Given $S(z)$, $\alpha(z)$, and $\Lambda(z)$, we can use Eq. (1.3) to calculate D(z) and then the required (z) distribution can be calculated through Eq. (1.4). In the case of a real and physically realizable active medium, the local gain distribution is a function of the pump and total signal intensity, as defined by the appropriate rate equations. Therefore, for a given pump power distribution, the choice of $S(z)$ implicitly defines $\alpha(z)$. The $D(z)$ variation is fully determined by the laser boundary conditions and defines the outputs at both laser ends as well as the device length.

In order to design a laser cavity that provides the maximum possible efficiency, we should first define the optimum $S(z)$. At any point in an active medium the energy transfer from pump to signal gives the local conversion efficiency, which when maximized results in a laser with ultimate efficiency. The net signal generated per unit length $\Delta S = 2\alpha(z)S(z)$ and the absorbed pump per unit length $\Delta P = 2\alpha_p(z)P(z)$ where α_p is the absorption coefficient for pump field and P is the pump power. The local pump-to-signal conversion efficiency $\eta(S,P) = \Delta S(S,P)/\Delta P(S,P)$ is a function of signal S and pump intensity P and it is determined by the rate equations and various loss mechanisms of the active medium. This implies that for a given pump intensity P, there exists certain signal intensity S_{opt} such that the conversion efficiency η is maximum. Figure 1.6 shows (a) the S_{opt} and the corresponding optimum gain α and (b) the resultant generated signal (ΔS) and absorbed pump power (ΔP) for an Er^{3+}/Yb^{3+}-codoped fiber for pump powers up to 200 mW at 976 nm and signal wavelength at 1550 nm. Figure 1.6c shows the maximum expected efficiency (left) and

output power (right) for the ultimate efficiency design.The curves in Figure 1.6 can be considered as the master curves, which for a given active fiber enable the design of maximum efficiency DFB lasers. Firstly, the input pump power and pumping scheme are defined, then the spatial distributions of pump power $P(z)$, signal power $S_{opt}(z)$, and corresponding gain $\alpha(z)$ are calculated using the results of Figure 1.6 in an iterative way. Assuming a co-pumped configuration, $P(0)$ is launched from the left-hand side and the majority of the output signal power is expected to exit from the right-hand side. At $z=0$ we find $S_{opt}(0)$ and calculate $\Delta P(0)$. The pump power exiting the infinitesimal segment at δz is then $P(\delta z)=P(0)-\Delta P(0)\delta z$. This is used to calculate $S_{opt}(\delta z)$, $\alpha(\delta z)$, and $\Delta P(\delta z)$, and proceed to $z=2\delta z$. Repeating these steps until the pump power reduces to zero gives the entire spatial distributions $S_{opt}(z)$ and $\alpha(z)$ (see Figure 1.6a and b). $D(z)$ can then be calculated using Eq. (1.3).

The boundary conditions at $z=0$ require a sharp transition between the $S_{opt}(0)$ and the small unwanted output power. This results in an extremely large delta-like function κ at $z=0$, which is beyond any grating writing technology capability. Therefore, we should define a smooth, physically realizable transition between a relatively small $D(0)$ and S_{opt}. $S(z)$ in such transition regions can be described by a cosh(mz) function (shown by dashed line in Figure 1.7b), which can be shown to correspond to an almost constant (z) (see Figure 1.7c). We then calculate $D(z)$ and find the position $z=L$ where the second boundary condition for $D(L)$ is met, giving the total device length. In the

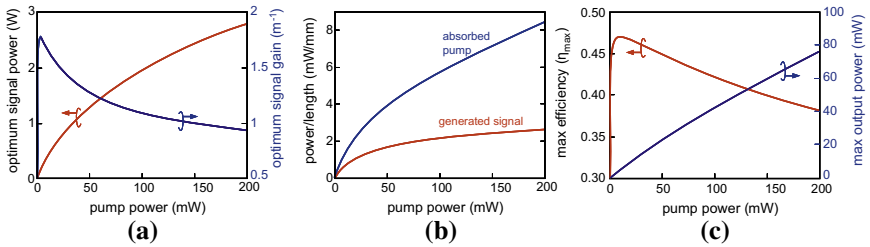

FIGURE 1.6 (a) Optimum signal power, (b) power extraction, and (c) maximum efficiency.

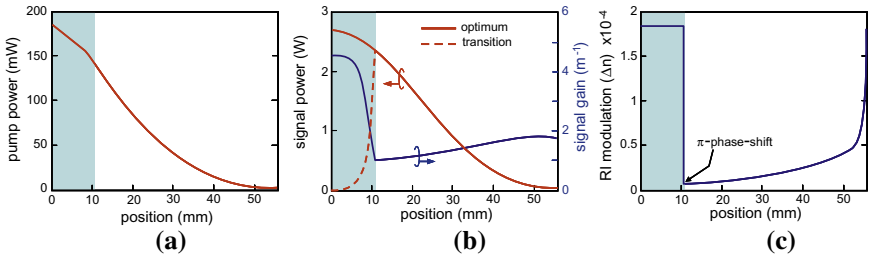

FIGURE 1.7 (a) Pump power, (b) signal power and local field gain, and (c) refractive index modulation as a function of position for a DFB laser with maximum efficiency.

co-directional pumping scheme $S_{opt}(L)$ is equal to the output power at $z = L$. Finally, substituting $S(z)$, $\alpha(z)$, $D(z)$ in Eq. (1.1) we can calculate the required apodization profile $\kappa(z)$, as shown in Figure 1.7c.

The grating apodization profile will depend on the pumping direction also as this will change the balance between optimum pump and signal distributions. Figures 1.8a and b show the refractive-index modulation profile for counter- and bi-directional pumping, respectively, for the same total pump power of 185 mW at 977 nm. It is shown that the pump direction affects the required optimum design, with the counter- and bi-directional designs requiring longer active fiber lengths and the bi-directional pumping scheme requiring three π-phase-shifts. Figure 1.8c compares the signal output power as a function of pump power for the three inverse-engineered DFB laser designs and contrasts them to the uniform, asymmetric π-phase-shifted configuration of the same active fiber length. It is shown that using the new designs, co-directional pumping results in a slightly smaller efficiency because it requires the largest unoptimized transition region. Bi-directional pumping, on the other hand, results in the best efficiency because the available pump power is split equally between the two ends. Smaller local pump intensities result in higher local efficiencies, with a positive net effect on the overall efficiency. All output power curves are shown to be very linear up to the design pump power of ~185 mW after which they start to saturate.

Figure 1.9a compares the experimental and simulation results for the 45 mm-long new design with a co-pumped 50 mm-long standard optimized design. Under the same operating conditions, a dramatic 57% increase in output power and efficiency is achieved. The new design is 10% shorter, shows a reduced threshold, and provides 63 mW of output signal power with 230 mW of pump power. This we believe is the highest output power for the shortest fiber DFB length reported to date. The standard optimized design uses the pump power less efficiently (see Figure 1.9b) and starts rolling off at ~30 mW of output power. At the design pump power of 185 mW, the experimentally observed efficiency of 33% compares very well with the theoretical efficiency limit of 39%. This deviation is due to the non-optimized transition region at the input, imposed by the grating writing constraints.

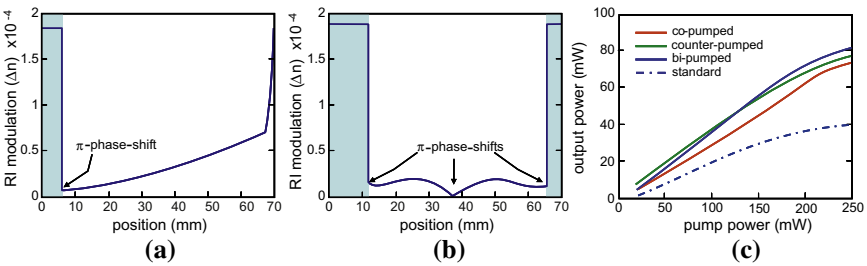

FIGURE 1.8 Inverse-engineered designs with (a) counter pumping, (b) bi-directional pumping, and (c) output power comparison.

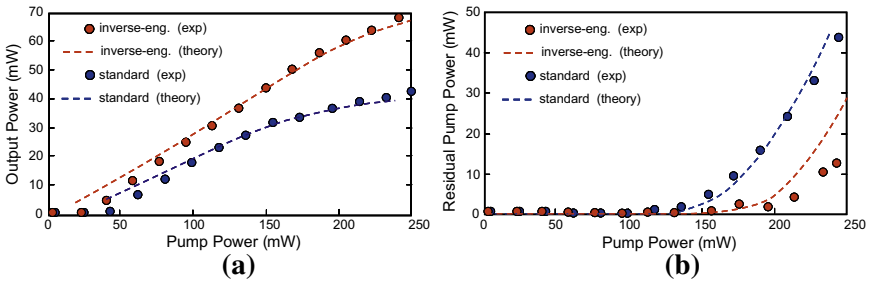

FIGURE 1.9 Comparison of (a) output powers and (b) residual pump powers from standard and new design DFB lasers (adapted from [19]).

It is also observed that the input/output linearity deteriorates and residual pump increases above the 185 mW design pump level. The new design operated in a single longitudinal mode and showed ~25 dB output power directionality at all the pump power up to 250 mW.

1.2.3 Optical performance of fiber DFB lasers

The effective integration of laser sources in high-performance systems/subsystems depends on a number of characteristics, such as polarization and wavelength stability as well as phase/frequency noise and/or relative intensity noise (RIN). These performance characteristics can be controlled accurately by proper fiber design.

1.2.3.1 Output power/polarization

The control of output signal polarization is extremely important since advanced lasers are invariably interfaced with a number of polarization-sensitive devices, such as modulators, isolators, and filters. The output polarization of fiber DFB lasers can be influenced by a number of fiber and cavity parameters, such as fiber birefringence and twist, polarization-dependent grating strength and/or phase shift as well as grating chirp [21,22]. The polarization mode competition and overall performance are influenced by the magnitude of the resulting polarization hole-burning and the local as well as global spatial hole-burning effects.

Figure 1.10a and b shows the normalized grating strength requirements as a function of polarization-dependent grating strength difference and phase-shift difference, respectively, in order to achieve single polarization operation. In this case, $\Delta\kappa = \kappa_x - \kappa_y$ is the grating strength difference along the x and y polarizations, $\Delta\phi = \Delta\phi_y - \pi$ is the phase error in the y-polarization alone, while always $\Delta\phi_x = \pi$. It is shown that in the absence of sufficient grating strength difference and/or phase-shift difference, the fiber DFB lasers operate in two polarizations. It is also shown that the stronger the fiber grating, the larger the required $\Delta\kappa$ and $\Delta\phi$ in order to achieve single polarization operation. The behavior in the presence of fiber twist is

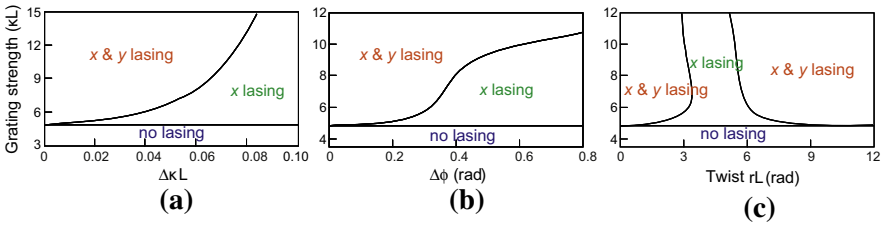

FIGURE 1.10 Polarization characteristics of fiber DFB lasers (adapted from [21,22]).

more complicated. Figure 1.10c shows a "window" of single polarization operation for moderate fiber twist, with dual polarization operation on either side. The width of the single polarization window depends on the grating strength.

Single polarization operation has been achieved by a number of techniques, such as twisting ordinary low-bi fibers [23], controlled UV exposure resulting in polarization-dependent phase shift and/or grating strength [24–27], or controlled-polarization back-reflection injection locking [28]. In most applications, single polarization DFB lasers are required to be subsequently spliced to hi-bi passive fibers in order to maintain polarization. Birefringent axes in hi-bi fibers, on the other hand, are known to rotate along the fiber length, with different rotation rates. It has been shown that single-mode, single-polarization fiber DFB lasers written directly in active hi-bi fibers exhibit elliptical polarization output. This is primarily due to inherent internal, frozen-in birefringence-axes rotation in hi-bi fibers. In this case, application of external birefringence-axes twist can be used to manipulate and control accurately the output state of polarization.

Figure 1.11a shows the schematic of a hi-bi fiber DFB laser, spliced to a matching passive hi-bi fiber. The passive fiber was angle-cleaved to minimize back-reflections. A quarter-wave plate and a high extinction ratio polarizer were used at the output in order to measure the polarization extinction ratio of the collimated laser output. The

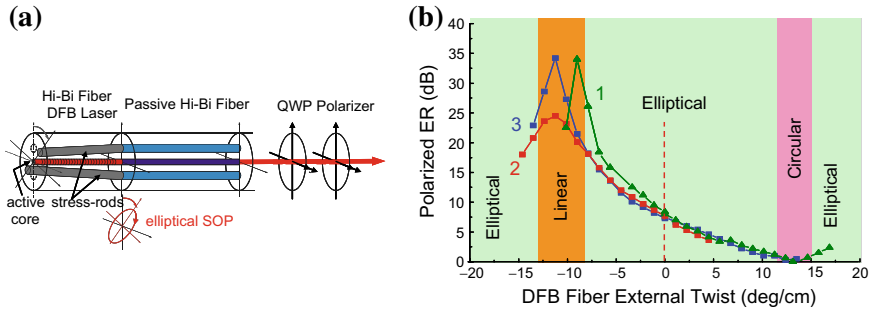

FIGURE 1.11 (a) Twisted fiber DFB laser characterization set-up, (b) PER as a function of DFB fiber twist [29].

polarization extinction ratio is defined as the max/min throughput power ratio (in dB), corresponding to two orthogonal polarizer orientations.

The active hi-bi fiber under test was measured to have an average internal axis twist of about +6°/cm. Figure 1.11b shows the output polarization extinction ratio (PER) as a function of applied DFB fiber external twist. Without any external twist, the PER was ~10 dB, which corresponds to an elliptical SOP. For twist rates of about −10 to −12°/cm the output SOP became linear, with max PER of ~35 dB. It is worth noting that the external twist required to achieve maximum PER is about two times the internal one. This is probably required in order to counteract the effect of the extra twist-induced stresses in addition to the initial geometrical twist. For opposite external twist rates of about +12°/cm the PER was ~0 dB, which corresponds to circular output SOP. For larger external twists, the PER is shown to increase again. This demonstrates an effective way of controlling and aligning the fiber DFB laser output SOP. It also shows that twisted hi-bi fiber DFB lasers can be potentially used as optical twist sensors.

1.2.3.2 Wavelength coverage

An advantage of fiber lasers in general is their ability to emit over broad bandwidths in different spectral regions by simply using different active dopants and slightly varying glass host compositions.

Using advanced grating writing techniques, the wavelength of operation in fiber DFB lasers is set by the Bragg grating period to <50 pm accuracy. Figure 1.12 shows the outputs of different π-phase-shifted fiber DFB lasers covering the entire C band. The fiber core is Er^{3+}/Yb^{3+}-codoped and the grating was written in a photosensitive boron codoped germano-silicate ring. The typical output power was 10 dBm and the wavelength stability was better than 0.14 nm over 70 °C. The optical signal-to-noise ratio, with 0.1 nm resolution, was better than 70 dB. L-band coverage has also been demonstrated using very strong, asymmetric π-phase-shifted gratings in high gain Er^{3+}-doped fibers [30,31]. Single-frequency, single-polarization outputs with power

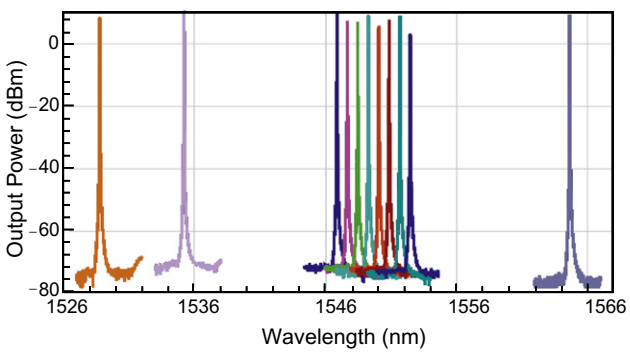

FIGURE 1.12 Er^{3+}/Yb^{3+} **fiber DFB laser wavelength coverage in the C-band.**

in excess of 80 mW were demonstrated with 980 nm pumping. These devices showed a rather large threshold of 16–20 mW.

In addition to more traditional Er^{3+} or Er^{3+}/Yb^{3+} fiber DFB lasers operating at telecom related wavelengths, fiber DFB lasers have also been demonstrated in Yb^{3+}-doped fibers operating at 970 nm [32] and in the 1.0 μm window [33], as well as thulium-doped fibers emitting in the 1735 nm [34] to 1943 nm [35] wavelength range. Fiber DFB lasers using Brillouin [36] and Raman amplification as the gain mechanism have also been demonstrated [37–39], opening up the possibilities for single-frequency sources in extended wavelength ranges not covered by active dopants. In addition to core pumping, cladding-pumped fiber DFB lasers have also been demonstrated as a means of scaling up the output power to 160 mW and simplifying the pumping configuration [40].

Typically Er^{3+} or Er^{3+}/Yb^{3+} are pumped at the 976–980 nm Er^{3+} and Yb^{3+} pump absorption peaks to keep the total length to a minimum. Pumping at the 520 nm [14] and 1480 nm Er^{3+} absorption bands has also been demonstrated. More complex intracavity pumping schemes have also been used for more efficient use of the pump power [41].

1.2.3.3 Linewidth and RIN performance

In addition to single stable longitudinal mode, showing no mode hopping, and single polarization output fiber DFB lasers show extremely narrow optical linewidth. Typical variation of the measured linewidth with increasing pump power is shown in Figure 1.13a for a 5 cm-long Er^{3+}/Yb^{3+} uniform, asymmetric fiber DFB laser pumped with an FBG-stabilized pump diode at 976.8 nm. The optical linewidth was measured using a delayed self-heterodyned interferometer with 5 km optical path imbalance.

At low pump powers, a linewidth of ~16 kHz is measured, but instead of the expected $1/P_{out}$ dependence, the linewidth increases with pump power. It has been shown that two noise sources are mainly responsible for the observed behavior, namely fundamental thermal noise at low pump power levels and temperature fluctuations induced by pump intensity noise at higher powers [42]. Potential techniques

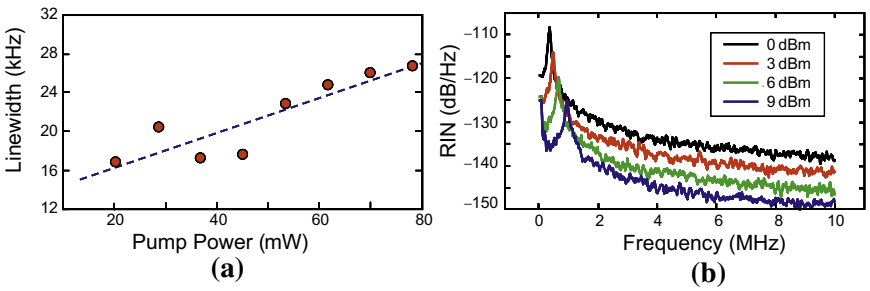

FIGURE 1.13 (a) Linewidth variation with pump power and (b) RIN for different output signal powers.

to overcome these limitations are the usage of a low noise pump or materials with a temperature-insensitive refractive index, e.g. by using specially tailored phosphate glasses. This has the added advantage of reducing both the pump fluctuation-induced linewidth broadening and the fundamental thermal noise. Varying the length of the grating, while keeping the grating strength constant, also modifies the fundamental thermal noise. Similarly, the fiber core radius can be enlarged to increase the mode volume and thereby decrease the thermal effects. Another approach to reduce the linewidth deterioration by pump noise is to use the DFB laser at low power in a master oscillator power amplifier (MOPA) to boost the power.

The relative intensity noise (RIN) measurement is plotted in Figure 1.13b for different signal output powers. It is shown that the RIN reduces as the output power increases and approaches −150 dB/Hz beyond 10 MHz. This is accompanied by a very low peak RIN of −125 dB/Hz at the relaxation frequency of 1 MHz. This is achieved without the added complication of feedback noise-reduction circuits.

Using a low concentration Er^{3+}-doped fiber, an asymmetric DFB laser has been demonstrated with sub-kHz (∼250 Hz) linewidth, without applying any external stabilization technique. The DFB laser length was 17 mm and the phase shift was introduced by UV post-processing. Due to short length and low Er^{3+} concentration, however, the laser showed relatively low optical efficiency [43].

1.2.3.4 Phase/frequency noise performance

As already mentioned, optical phase is used lately to encode data in advanced optical communications systems, resulting in record spectral efficiencies [44]. The phase characteristics of optical sources are also shown to play an important role in a number of other advanced applications, such as high-performance interferometric optical sensors, ultrasensitive interferometer-based phase measurements in optical component response, and ultrahigh resolution optical spectroscopy. In all the aforementioned applications the absolute frequency stability, spectral linewidth, and spectrally/temporally dependent phase/frequency noise characteristics of the lasers used are critical to understanding/optimizing the system performance. Theoretical studies have predicted that the phase noise and linewidth of the laser source can affect significantly the transmission penalties in coherent-optical systems [45,46].

Figure 1.14a shows the frequency noise spectrum of a free-running fiber DFB laser compared to other laser sources [47,48]. The theoretical thermal noise floor of a 10 mm-long fiber cavity is shown as a dashed line. Measured noise levels for other commonly used laser sources, such as a Nd:YAG ring laser, a Hitachi HLP 1400 semiconductor laser, and a commercial semiconductor DFB laser with 1.6 MHz linewidth, are included for comparison. The estimated frequency noise level of a bulk glass Er^{3+}/Yb^{3+} laser is indicated with a diamond. Figure 1.14b compares the frequency noise spectrum of commercially available fiber DFB (Basik) with the ones of a fiber-based Fabry-Perot laser (ROCK), a hybrid integrated-optics/semiconductor laser (RIO), and a virtual-ring waveguide laser (Orbit) [49]. It is shown that the fiber DFB and the virtual-ring waveguide lasers show better frequency noise performance, with the fiber laser having the edge especially at low frequencies.

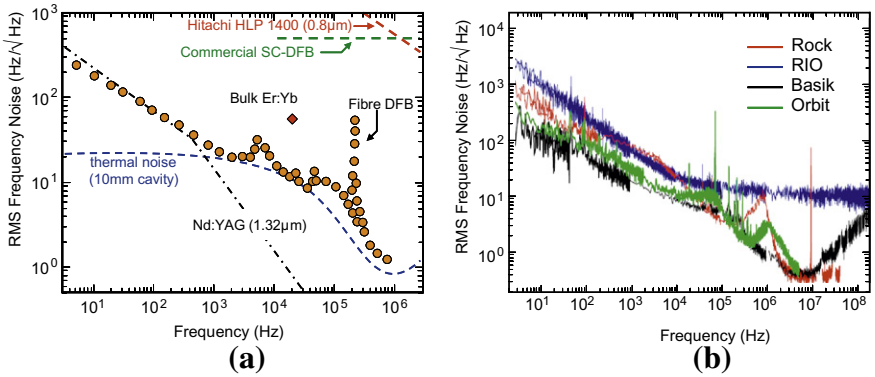

FIGURE 1.14 RMS frequency noise measurements (a) of a free-running fiber DFB laser [48] and (b) comparison of commercially available lasers [49].

A fundamental source of laser frequency noise is the thermodynamically defined thermal energy within the fiber. For a fiber DFB laser with a 1 cm-long effective cavity length, the expected thermal noise floor decreases from about 25 dBHz/$\sqrt{\text{Hz}}$ at 1 kHz to about -5 dBHz/$\sqrt{\text{Hz}}$ at 1 MHz. Below 50 kHz the noise increase above the thermal noise floor is believed to be caused by acoustical vibrations. Above 1 kHz and away from the relaxation oscillation frequency (f_{ro}), the measured frequency noise floor varies from 0 to 6 dB above the expected thermal noise floor. The origin of excess frequency noise above $f = 50$ kHz is not understood in detail. The use of longer cavities is proven to lower the frequency noise contribution from fundamental thermal fluctuations, and therefore the previously mentioned step-apodized and inverse-engineered designs, characterized by substantially longer effective cavities, are expected to show lower frequency noise. For frequencies below 1 kHz the rms frequency noise follows a $1/f$ dependence, the origin of which has not been fully identified. Around f_{ro} the optical frequency noise and RIN are found to be strongly interrelated and associated by the linewidth enhancement factor [47].

1.2.3.5 Tunability

Tunable lasers are of paramount importance in modern telecom systems as they can be used to populate different channel slots and reduce laser inventory. In addition, they can also provide a route to reconfigurable WDM systems. The response times are in the 0.1 ms–1 s range, depending on the actuator and tuning mechanism utilized. The lower limit is imposed by the acoustic velocity of strain waves in the fibers. Fiber DFB lasers can be tuned effectively by heating, stretching, and/or compressing uniformly the grating cavity. Continuous tuning over 27 nm has been demonstrated in Er^{3+}/Yb^{3+} all-fiber, DFB lasers using a simple tuning mechanism for axial extension and compression. The demonstrated devices operated with powers up to 10 dBm and remain operating in single mode over the full tuning range [50].

1.2.3.6 Power scaling—master-oscillator power amplifiers (MOPAs)

Optimized step-apodized and inverse-engineered designs provide maximum efficiency and output powers in the 10s of mW range. Higher powers are potentially needed if the output of a single DFB laser is to be split in multiple channels. Also, output powers should be scaled up to higher levels, in order to make fiber DFB lasers suitable for medical and other industrial applications. A single-frequency narrow-linewidth laser at 1552 nm was demonstrated with an output power of 83 W using a MOPA configuration. A fiber DFB seed laser with a linewidth of 13 kHz was polarization scrambled, in order to avoid the onset of SBS, and boosted through a chain of fiber amplifiers [51]. Using a MOPA configuration, the output of an Yb^{3+}-doped all-fiber DFB laser was boosted to 400 mW [52]. The DFB fiber laser was pumped by a 976 nm amplified spontaneous emission (ASE) source based on an Yb^{3+}-doped jacketed-air-clad fiber pumped by a 915 nm multimode laser diode source. The total output power response was approximately linear and the overall performance was limited by the available pump power. The spectral characteristics and signal-to-noise ratio remained similar to the master-oscillator DFB laser over the entire output power range.

1.2.4 Multi-wavelength fiber DFB lasers and fiber DFB laser arrays

In addition to single-wavelength outputs, fiber DFB lasers can be designed to provide multi-wavelength outputs. Moire-type fiber DFB lasers operating simultaneously on two-wavelength channels around 1.55 μm at room temperature have been realized. The demonstrated lasers have channel separations of 25, 50, and 100 GHz with identical output powers of 1 mW [53]. Multi-wavelength fiber lasers were also obtained by writing two superimposed chirped fiber 8 cm-long Bragg gratings in a photosensitive Er^{3+}/Yb^{3+}-codoped optical fiber. The chirped gratings create a distributed Fabry-Pérot structure in which the resonating fields of the different laser lines are spatially separated, thus, reducing gain cross-talk. Multi-wavelength lasers emitting simultaneously over 8 and 16 lines spaced by 50 GHz have been demonstrated [54].

Despite their simplicity, in multi-wavelength DFB laser sources all channels are intertwined and co-exist inside the fiber cavity. Although this might be beneficial for sensor applications, possible use in telecom systems requires separation and individual access of all the different channels. To this end, fiber DFB laser arrays with pump redundancy have been demonstrated [55]. Figure 1.15a shows a schematic of the 16-channel transmitter module. This module consists of eight pump diodes, a pump redundancy unit, and sixteen 5 cm-long asymmetric fiber DFB lasers with isolators on the output end. The pump redundancy module splits the powers from the pumps equally between the fiber DFB lasers, such that each laser still receives the pump power corresponding to that provided by one pump diode. The particular module is made up of twenty 2×2 3 dB couplers at 980 nm and splits equally the eight inputs to 16 outputs. The total insertion loss for each pump input channel in this 16-channel module is ~1.5 dB.

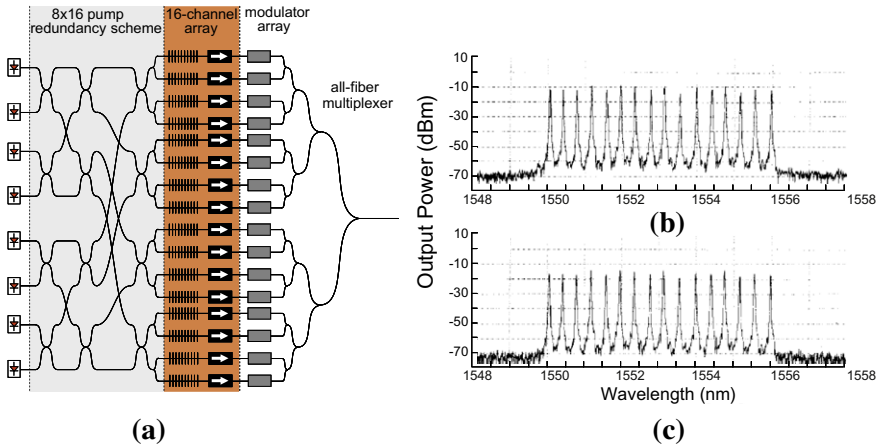

FIGURE 1.15 (a) Schematic of 16-channel fiber DFB laser array with pump redundancy. 50 GHz WDM transmitter module output with (b) all pumps, (c) four pumps only [55].

Sixteen fiber DFB lasers separated in frequency by 50 GHz were fabricated, operating in a single polarization mode with a purity of 40 dB and with a single-sided output power ratio of 50:1. The slope efficiency of the lasers was ~25% and using the pump redundancy scheme with 50 mW power from each pump diode resulted in output powers of about $-10\,\text{dBm} \pm 0.25\,\text{dBm}$ for all channels. The outputs of the 16 lasers were combined in an all-fiber multiplexer consisting of fifteen 1550 nm 3 dB splitters with a total insertion loss of ~10 dB. Noise measurements on the individual channels showed RIN < -160 dB/Hz for frequencies above 10 MHz and RIN < -165dB/Hz for frequencies larger than 30 MHz, indicating performance well suited for high-speed communication systems.

DFB fiber laser arrays with one shared pump have also been used as cost-effective and wavelength selectable optical sources. A large number of wavelengths can be selected via optical space switches, and this system is a good candidate for use as a wavelength selectable, backup transmitter for wavelength division multiplexed (WDM) systems [56].

1.2.5 Optical transmission system experiments

Fiber DFB lasers have been used successfully in a number of optical transmission system experiments. A DFB fiber laser operating at 1607 nm having 75.4 dB OSNR and RIN below -150 dB/Hz was used in a 10 Gbit/s transmission experiment over 72 km of standard single mode fiber with no observable difference when compared to an external-cavity semiconductor source [30].

WDM transmission and dispersion compensation at 40 Gbit/s over 200 km standard fiber has been demonstrated on a 100 GHz grid using four high-power

single-polarization single-sided output fiber DFB laser-based transmitters and a single four-channel WDM chirped fiber-Bragg grating dispersion compensator [57]. In-line fiber DFB lasers have also been used as orthogonally polarized pump sources to provide phase conjugation, by fiber four-wave mixing, and spectral inversion for efficient mid-span dispersion compensation in optical links. This technique provides polarization-independent operation in a simple all-fiber configuration without the need for externally injected pumps [58].

Finally, fiber DFB lasers can be used in microwave photonics applications. Dual polarization mode fiber DFB lasers fabricated in an elliptical-core Er-doped fiber have been used for efficient 40 GHz optical millimeter wave generation with 3 dB beat linewidth of 900 Hz [59]. Such millimeter-wave sources can be advantageous for applications involving phased-array antennas or fiber-fed radio systems.

1.2.6 Fiber DFB laser in non-telecom applications

Due to the unique combination of output power and polarization stability, narrow linewidth and extremely low intensity and phase/frequency noise, fiber DFB lasers have already found widespread usage outside the telecom field. It should be first emphasized that the only laser in the National Ignition Facility (NIF), the largest laser system in the world, is a fiber DBF laser [60]. The 1.8 MJ energy, 500 MW peak power at the output of the NIF laser system starts from a single-fiber DFB oscillator, before it splits in 192 chains of multiple solid-state high-power amplifiers. The Yb-doped oscillator produces ~20 mW of output power at 1053.01 ± 0.01 nm in a single longitudinal mode when pumped with 130 mW from a 980 nm laser diode.

Fiber DFB lasers have been used in a number of sensor applications such as high-performance seeds for sensor arrays [61] enabling remote measurements from a large-scale interferometric optical sensor system, using a 500km optical transmission link between interrogator and sensor array. A phase noise floor of −80 dB re 1 rad/$\sqrt{\text{Hz}}$ peak was achieved (equivalent to 1 mPa/$\sqrt{\text{Hz}}$).

DFB fiber lasers have also been used as the sensing elements [62]. Radio-frequency (RF) beat frequencies between two longitudinal modes and two polarization modes of a birefringent dual-longitudinal-mode moire distributed-feedback fiber laser have been employed to measure strain and temperature simultaneously. Operating entirely in the RF domain, this approach potentially allows one to employ low-cost and precise RF measuring techniques. The achieved sensor accuracy was $\pm 15\,\mu\varepsilon$ and $\pm 0.2\,^{\circ}\text{C}$ [63]. They have also been used as sensors to characterize temperature distribution along other DFB lasers [64].

1.3 SUMMARY AND CONCLUDING REMARKS—OUTLOOK

This chapter has reviewed the latest developments in high-performance fiber lasers, and their potential use in modern high spectral efficiency coherent optical communication systems. We have presented results on asymmetric, step-apodized, and

inverse-engineered fiber DFB laser designs with high ultimate efficiency. We have also discussed the output power scalability, wavelength coverage, tunability, polarization properties, output power stability and linewidth, as well as frequency noise characteristics of these lasers.

It has been shown that modern optical communication systems using nonbinary modulation formats and coherent detection provide maximum spectral efficiency and improve tolerances to other transmission impairments [65]. In has been predicted that compared to other coherent schemes, 16-QAM modulation with coherent detection results in 4 bits/symbol efficiency with minimum possible optical signal-to-noise-ratio (OSNR) requirements. However, in coherent optical systems the increased sensitivity to phase noise and frequency stability sets extremely stringent requirements on laser oscillator linewidth. It has also been shown that other effects, like dispersion-enhanced phase noise, induce severe degradations to advanced optical systems performance, such as CO-OFDM [47]. In this case, to reduce the OSNR requirements for transmission of 56 Gbaud DP-QPSK (224 Gb/s) over 3200 km requires lasers with linewidth of a few 10–100 kHz. Undoubtedly, transmission over longer distances and higher repetition rates will further increase the requirements on laser linewidth and phase noise. We have shown that fiber DFB lasers can exhibit record sub-kHz linewidth without the need of external controls and offer themselves as cheap and versatile replacements of currently used expensive and complicated external-cavity semiconductor counterparts [66]. We have also shown frequency noise comparison showing superior fiber DFB laser performance over other fiber and semiconductor lasers, especially in the low frequency regime. This feature is proving to be particularly advantageous in other photonic applications, such as interferometric sensor arrays.

Although fiber lasers show a number of advantages over other technologies in terms of linewidth, phase noise, power scalability, stability, and simplicity more research is required to address the remaining issues affecting the ultimate linewidth limits and phase noise performance. Work is required to further understand the impact of host material and cavity design, output power level, and pump characteristics on the aforementioned fundamental limits. Also more effort is needed to study the parameters that affect the single polarization performance and polarization control. Finally, further work should be carried out on alternative gain mechanisms such as Raman and Brillouin DFBs to increase the wavelength coverage.

References

[1] M. Nakazawa, T. Hirooka, M. Yoshida, K. Kasai, Ultrafast coherent optical transmission, J. Sel. Top. Quant. Electron. 18 (2012) 363.
[2] S.L. Jensen, I. Morita, H. Tanaka, 10 Gb/s OFDM with conventional DFB lasers, ECOC, Paper Tu.2.5.2 2007.
[3] W-R. Peng, Analysis of laser phase noise effect in direct-detection optical OFDM transmission, J. Lightwave Technol. 28 (2010) 2526.
[4] M. Nakazawa, Recent progress on ultrafast/ultrashort/frequency-stabilized erbium-doped fiber lasers and their applications, Front. Optoelectron. China 3 (2010) 38.

[5] H. Kogelnik, C.V. Shank, Stimulated emission in a periodic structure, Appl. Phys. Lett. 18 (1971) 152.
[6] H. Kogelnik, C.V. Shank, Coupled-wave theory of distributed feedback lasers, J. Appl. Phys. 43 (1972) 2327–2335.
[7] M. Nakamura, A. Yariv, H.W. Yen, S. Somekh, H.L. Garvin, Optically pumped GaAs surface laser with corrugation feedback, Appl. Phys. 22 (1973) 515.
[8] D.R. Scifres, R.D. Burnham, W. Streifer, Distributed feedback single heterojunction GaAs diode laser, Appl. Phys. Lett. 25 (1974) 203.
[9] H.A. Haus, C.V. Shank, Antisymmetric taper of distributed feedback lasers, J. Quant. Electron. 12 (1976) 532.
[10] K. Utaka, S. Akiba, K. Sakai, Y. Matsushima, λ/4-shifted InGaAsP/InP DFB lasers, J. Quant. Electron. 22 (1986) 1042.
[11] J.T. Kringlebotn, J.L. Archambault, L. Reekie, D.N. Payne, "Er^{3+}-Yb^{3+}-codoped fiber distributed-feedback laser, Opt. Lett. 19 (24) (1994) 2101.
[12] M. Sejka, P. Varming, J. Hubner, M. Kristensen, Distributed-feedback Er^{3+}-doped fiber laser, Electron. Lett. 31 (1995) 1445.
[13] W.H. Loh, R.I. Laming, 1.55 μm phase-shifted distributed feedback fiber laser, Electron. Lett. 31 (1995) 1440.
[14] W.H. Loh, S.D. Butterworth, W.A. Clarkson, Efficient distributed feedback erbium-doped germanosilicate fiber laser pumped in 520 nm band, Electron. Lett. 32 (1996) 2088.
[15] G. Meltz, W.W. Morey, W.H. Glenn, Formation of Bragg gratings in optical fibers by a transverse holographic method, Opt. Lett. 14 (1989) 823.
[16] M.J. Cole, W.H. Loh, R.I. Laming, M.N. Zervas, S. Barcelos, Moving fibre/phase mask-scanning beam technique for enhanced flexibility in producing fibre gratings with a uniform phase mask, Electron. Lett. 31 (1995) 1488.
[17] S.J. Mihailov, C.W. Smelser, D. Grobnic, R.B. Walker, L. Ping Lu, D. Huimin, J. Unruh, Bragg gratings written in all-SiO_2 and Ge-doped core fibers with 800-nm femtosecond radiation and a phase mask, J. Lightwave Technol. 22 (2004) 94.
[18] K. Yelen, L.M.B. Hickey, M.N. Zervas, A new design approach for fiber DFB lasers with improved efficiency, J. Quant. Electron. 40 (2004) 711.
[19] K. Yelen, M.N. Zervas, L.M.B. Hickey, Fiber DFB lasers with ultimate efficiency, J. Lightwave Technol. 23 (2005) 32.
[20] W.H. Loh, B.N. Samson, L. Dong, G.J. Cowle, K. Hsu, High performance single frequency fiber grating-based erbium:ytterbium-codoped fiber laser, J. Lightwave Technol. 16 (1998) 114.
[21] E. Ronnekleiv, M.N. Zervas, J.T. Kringlebotn, Modeling of polarization mode competition in fiber DFB lasers, J. Quant. Electron. 34 (1999) 1559.
[22] E. Ronnekleiv, M.N. Zervas, J.T. Kringlebotn, Corrections to modeling of polarization mode competition in fiber DFB lasers, J. Quant. Electron. 35 (1999) 1097.
[23] Z.E. Harutjunian, W.H. Loh, R.I. Laming, D.N. Payne, Single polarization twisted DFB laser, Electron. Lett. 32 (1996) 346.
[24] L.B. Fu, M. Ibsen, P.W. Turner, D.J. Richardson, D.N. Payne, Keyed axis single-polarization all-fiber DFB laser, Electron. Lett. 38 (2002) 1537.
[25] H. Storøy, B. Sahlgren, R. Stubbe, Single polarization fiber DFB laser, Electron. Lett. 33 (1997) 56.
[26] J.I. Philipsen, M.O. Berendt, P. Varming, V.C. Lauridsen, J.H. Povlsen, J. Hübner, M. Kristensen, B. Pálsdóttir, Polarization control of DFB fiber laser using UV-induced birefringent phase-shift, Electron. Lett. 34 (1998) 678–679.

[27] M. Ibsen, E. Rønnekleiv, G.J. Cowle, M.O. Berendt, O. Hadeler, M.N. Zervas, R.I. Laming, Robust high-power (>20 mW) all-fiber DFB lasers with unidirectional and truly single polarization outputs, in: Proceedings of the Conference on Lasers and Electro-Optics (CLEO) 1999, Baltimore, MD, 1999, CWE4, p. 245.
[28] S. Yamashita, G.J. Cowle, Single-polarization operation of fiber distributed feedback lasers by injection locking, J. Lightwave Technol. 17 (1999) 509–513.
[29] M.N. Zervas, R. Wilmshurst, L.M.B. Walker, Twisted Hi-Bi fiber DFB lasers with controllable output polarization, in: Proceedings of the Conference on Lasers and Electro-Optics (CLEO), Paper CF3N.5, 2012.
[30] H.N. Poulsen, P. Varming, A. Buxens, A.T. Clausen, I. Munoz, P. Jeppesen, C.V. Poulsen, J.E. Pedersen, L. Eskildsen, 1607 nm DFB fibre laser for optical communications in the L-band, in: European Conference on Optical Communication, ECOC '99, Nice, France, September 1999, Paper MoB2.1.
[31] P. Varming, V.C. Lauridsen, J.H. Povlsen, J.B. Jensen, M. Kristensen, B. Palsdottir, Design and fabrication of Bragg grating based DFB fiber lasers operating above 1610 nm, in: Optical Fiber Communication Conference, OSA Technical Digest Series (Optical Society of America, 2000), Paper ThA6.
[32] L.B. Fu, M. Ibsen, D.J. Richardson, D.N. Payne, 977-nm all-fiber DFB laser, Photon. Technol. Lett. 16 (2004) 2442.
[33] A. Asseh, H. Storøy, J.T. Kringlebotn, W. Margulis, B. Sahlgren, S. Sandgren, R. Stubbe, G. Edwall, 10 cm Yb^{3+} DFB fibre laser with permanent phase shifted grating, Electron. Lett. 31 (1995) 969.
[34] S. Agger, J. Hedegaard Povlsen, P. Varming, Single-frequency thulium-doped distributed-feedback fiber laser, Opt. Lett. 29 (2004) 1503.
[35] Z. Zhang, D.Y. Shen, A.J. Boyland, J.K. Sahu, W.A. Clarkson, M. Ibsen, High-power Tm-doped fiber distributed-feedback laser at 1943 nm, Opt. Lett. 33 (2008) 2059.
[36] K.S. Abedin, P.S. Westbrook, J.W. Nicholson, J. Porque, T. Kremp, X. Liu, Distributed feedback fiber laser employing Brillouin gain, in: Proceedings of the Conference on Lasers and Electro-Optics (CLEO), Paper CF3N, 2012.
[37] V.E. Perlin, H.G. Winful, Distributed feedback fiber Raman laser, J. Quantum Electron. 37 (2001) 38.
[38] Y. Hu, N.G.R. Broderick, Improved design of a DFB Raman fibre laser, Opt. Commun. 282 (2009) 3356.
[39] P.S. Westbrook, K.S. Abedin, J.W. Nicholson, T. Kremp, J. Porque, Raman fiber distributed feedback lasers, Opt. Lett. 36 (2011) 2895.
[40] A. Schülzgen, L. Li, D. Nguyen, Ch. Spiegelberg, R. Matei Rogojan, A. Laronche, J. Albert, N. Peyghambarian, Distributed feedback fiber laser pumped by multimode pump diodes, Opt. Lett. 33 (2008) 614.
[41] W.H. Loh, B.N. Samson, Z.E. Harutjunian, R.I. Laming, Intracavity pumping for increased output power from a distributed feedback erbium fiber laser, Electron. Lett. 32 (1996) 1204.
[42] P. Horak, N.Y. Voo, M. Ibsen, W.H. Loh, Pump-noise-induced linewidth contributions in dfb fiber lasers, Photon. Technol. Lett. 18 (2006) 998.
[43] A.C.L. Wong, W.H. Chung, H.Y. Tam, C. Lu, Ultra-short distributed feedback fiber laser with sub-kilohertz linewidth for sensing applications, Laser Phys. 21 (2011) 163.
[44] A.H. Gnauck, P.J. Winzer, Optical phase-shift-keyed transmission, J. Lightwave Technol. 23 (2005) 115.

[45] W. Shieh, K.-P. Ho, Equalization-enhanced phase noise for coherent-detection systems using electronic digital signal processing, Opt. Express 16 (2008) 15718.
[46] Q. Zhuge, M. Morsy-Osman, D.V. Plant, Analysis of dispersion-enhanced phase noise in CO-OFDM systems with RF-pilot phase compensation, Opt. Express 19 (2011) 24030.
[47] E. Ronnekleiv, Frequency and intensity noise of single frequency fiber Bragg grating lasers, Opt. Fiber Technol. 7 (2001) 206.
[48] E. Rønnekleiv, S.W. Løvseth, J.T. Kringlebotn, Er-doped fiber distributed feedback lasers: properties, applications and design considerations, Proc. SPIE 4943 (2003) 69.
[49] R. Slavik, Y. Liao, E. Austin, P. Petropoulos, D.J. Richardson, Full characterization and comparison of phase properties of narrow linewidth lasers operating in the C-band, in: 21st International Conference on Optical Fiber Sensors, Proc. SPIE, vol. 7753, 2011, p. 775338.
[50] M. Ibsen, S.Y. Set, G.S. Goh, K. Kikuchi, Broad-band continuously tunable all-fiber DFB lasers, Photon. Technol. Lett. 14 (2002) 21.
[51] C. Alegria, Y. Jeong, C. Codemard, J.K. Sahu, J.A. Alvarez-Chavez, L. Fu, M. Ibsen, J. Nilsson, 83-W single-frequency narrow-linewidth MOPA using large-core erbium-ytterbium co-doped fiber, Photon. Technol. Lett. 16 (2004) 1825.
[52] C.A. Codemard, L.M.B. Hickey, K. Yelen, D.B.S. Soh, R. Wixey, M. Coker, M.N. Zervas, J. Nilsson, 400 mW, 1060 nm ytterbium doped fiber DFB laser, Proc. SPIE, vol. 5335, 2004, p. 56.
[53] M. Ibsen, E. Ronnekleiv, G.J. Cowle, M.N. Zervas, R.I. Laming, Multiple wavelength all-fibre DFB lasers, Electron. Lett. 36 (2000) 143.
[54] R. Slavik, I. Castonguay, S. LaRochelle, S. Doucet, Short multiwavelength fiber laser made of a large-band distributed Fabry-Pérot structure, Photon. Technol. Lett. 16 (2004) 1017.
[55] M. Ibsen, S. Alam, M.N. Zervas, A.B. Grudinin, D.N. Payne, 8- and 16-Channel all-fiber DFB laser WDM 8- and 16-channel all-fiber DFB laser WDM, Photon. Technol. Lett. 11 (1999) 1114.
[56] X. Zheng, P.J.S. Pedersen, P. Varming, A. Buxens, Y. Qian, P. Jeppesen, Cost-effective wavelength selectable light source using DFB fibre laser array, Electron. Lett. 36 (2000) 620.
[57] M. Ibsen, A. Fu, H. Geiger, R.I. Laming, Fibre DFB lasers in a 4×10 Gbit/s WDM link with a single Sinc-sampled fibre grating dispersion compensator, in: 24th European Conference on Optical Communication, vol. 3, 20–24 September, 1998, pp. 107–111.
[58] S. Yamashita, S.Y. Set, R.I. Laming, Polarization independent, all-fiber phase conjugation incorporating inline fiber DFB lasers, Photon. Technol. Lett. 10 (1998) 1407.
[59] W.H. Loh, J.P. de Sandro, G.J. Cowle, B.N. Samson, A.D. Ellis, 40 GHz optical-millimeter wave generation with a dual polarization distributed feedback fiber laser, Electron. Lett. 33 (1997) 594.
[60] D.F. Browning, G.V. Erbert, Distributed feedback fiber laser: the heart of the national ignition facility, Report UCRL-ID-155446, 2003.
[61] E. Austin, P. Nash, Q. Zhang, S. Alam, M.N. Zervas, R. Slavik, P. Petropoulos, D.J. Richardson, 500 km remote interrogation of optical sensor arrays, Proc. SPIE 7753 (2011) 77532M.
[62] G.A. Cranch, G.M.H. Flockhart, C.K. Kirkendall, Distributed feedback fiber laser strain sensors, IEEE Sens. J. 8 (2008) 1161.

[63] O. Hadeler, M. Ibsen, M.N. Zervas, Distributed-feedback fiber laser sensor for simultaneous strain and temperature measurements operating in the radio-frequency domain, Appl. Opt. 40 (2001) 3169.
[64] O. Hadeler, M.N. Zervas, Application of a DFB fibre laser temperature sensor for characterizing pump induced temperature distributions along another DFB fibre laser, in: SPIE Proceedings of the International Conference on Optical Fiber Sensors, 4185, 2000, p. 142.
[65] J.M. Kahn, K.P. Ho, Spectral efficiency limits and modulation/detection techniques for DWDM systems, J. Sel. Top. Quant. Electron. 10 (2004) 259.
[66] E. Ip, J.M. Kahn, D. Anthon, J. Hutchins, Linewidth measurements of MEMS-based tunable lasers for phase-locking applications, Photon. Technol. Lett. 17 (2005) 2029.